Parallel Adaptive Method for Selecting Points of Interest in Structures: Cranial Deformation

Claudia García-Blanquel[1], Amitava Majumdar[2], and René Luna-García[1]

[1] Centro de Investigación en Computación, IPN, Mexico City, Mexico

[2] San Diego Supercomputer Center, University of California San Diego, La Jolla, CA 92037, USA

cgarciab10@sagitario.cic.ipn.mx, majumdar@sdsc.edu, lunar@cic.ipn.mx

Abstract. In this paper, we present a cranial deformation simulation by applying a stress model using the Finite Element Method (FEM). We determine the geometry of cranium by processing 134 Computed Tomography (CT) images. We implement an image segmentation algorithm to build a three-dimensional cranium structure. We simulate stress and propose the boundary conditions according to the final position of forces applied by a stereotactic frame fixed on the human head. We used probabilistic and adaptive methods to select points in the structure with the purpose of reducing the computational cost and computational error due to discretization problem. We implement the algorithms using parallel programming (PosixThread and MPI).

Keywords. HPC, parallel programming, FEM, adaptive method, cranial deformation.

Método adaptativo paralelo para la selección de puntos de interés en estructuras: deformación craneal

Resumen. En este trabajo, presentamos un modelo de deformación por esfuerzos para el cráneo humano usando el Método del Elemento Finito (FEM). Determinamos la geometría del cráneo a partir de 134 imágenes de tomografías computarizadas (CT) e implementamos un algoritmo para la segmentación de imágenes y construir una imagen tridimensional del cráneo. Simulamos los esfuerzos y proponemos las condiciones de frontera de acuerdo con la posición de la fuerza aplicada por un marco estereotáctico fijo sobre un cráneo humano. Aplicamos métodos probabilísticos y adaptativos para la selección de puntos en la estructura con la finalidad de reducir el costo computacional y el error de cálculo debido a la discretización del problema. Implementamos los algoritmos usando programación paralela (PosixThread y MPI).

Palabras clave. HPC, programación paralela, FEM, método adaptivo, deformación craneal.

1 Introduction

In science and engineering, models of continuous systems may contain a great number of degrees of freedom, so when they are discretized by a numerical method, the latter produces an algebraic system of linear equations, requiring a high computational cost. Therefore, parallel computing and High Performance Computing (HPC) are necessary resources that should be used in this context.

One of the great challenges of the scientific computing field is analysis of a series of considerations determined by factors external to the problem of interest, which impact directly on the way of implementing the solution of the problem. Some of these considerations are the number of available processors, size and type of the domain partition, default runtime.

These main considerations leave a numerical solution with few degrees of freedom, making computing application an efficient tool which also allows it to be flexible and adaptable to future specification changes, a common matter in science and engineering.

On the other hand, parallel computing is a technique which allows distribution of a large computing load among many processors. It is well

known [13] that one of the major difficulties of parallel computing is coordination of the activities of different processors and information exchange among them. The mathematical formulation of the problem, i.e., domain decomposition [1, 3], incorporates a natural separation of tasks and remarkably simplifies information transmission.

The models derived from the field of Biomechanics have been viewed as continuous models. Biomechanics corresponds to Mechanics applied to Biology, that is, the discipline intended to predict mechanics in living beings. This science helps to understand the usual functioning of organisms, to characterize the behavior of living tissues and organs from the mechanical viewpoint, to predict changes in function of certain alterations, and to propose methods of artificial interventions.

With this concept, the problem is posed within the Impact Biomechanics area, which looks for a better understanding of impacts on key anatomic areas, the circumstances under which a trauma is produced, and its frequency.

For these reasons, there is a growing interest in the use of detailed models for better representation. This implies a higher necessity for a feature detection task. For the representation of some entity, it is therefore necessary to be able to select distinctive points on a model in order to keep the efficiency in the processes applied on them. Some tasks that benefit from this capability are object registration [5], object retrieval and matching [6], mesh simplification, viewpoint selection [9] and mesh segmentation [12, 18], just to mention some.

The interest point selection on data is a challenging problem for several reasons. First, there is no consensus about definition of an interest point. A commonly used definition relates the measures of interest to the level of protrusion of outstanding local structures. So, vertices on smooth or nearly planar sections of a surface will have low interest, as opposite to vertices in regions with uncommon local structure. For instance, in a cranium-shaped model, an interest point selection should select vertices on the scalp and face. Second, the topology meshes are arbitrary. That is, a vertex can have an arbitrary number of neighboring vertices. This makes the task of selecting a local neighborhood around a vertex harder. In addition, this drawback causes such effect that different tessellations may represent the same locality and therefore the interest point method should be able to deal with that. Third, without a well-defined topological structure for meshes, the extent of a locality in which a vertex is an interest point is unknown or difficult to compute. Finally, there is no additional information other than the position of vertices and the connectivity information among them. This fact complicates the process because the level of interest needs to be measured using available information, which also depends on the topology of the mesh.

We use a parallel adaptive method for selection points of interest on structures. We chose the gradient operator for several reasons. First, the computation of the operator is an efficient and simple task. This is an important issue if we want to use the interest point selection as a preliminary stage of subsequent process such as cranial deformation. Second, the gradient method has been effectively used in a number of applications which have shown high effectiveness as reported in publications [21, 17]. Finally, interesting evidence has been found recently, which greatly favors the ability to capture concavities, flexibility of tailoring the force field, and reduction of computational cost [19, 20].

The overall process consists of three steps: reduce computational time, improve accuracy, and present an analysis of the structure to observe deformities due to application of stress using a different set of interest points.

2 Image Processing

The original measurement protocol included high-resolution images (*512x512* pixel matrix) with a slide increment of 0.47 mm. In the first step, in order to construct the geometric model of the cranium, outer bone contours were extracted, slice per slice, from the stack of 134 CT (Computed Tomography).

$$\text{TC value} = \frac{\mu - \mu_{\text{agua}}}{\mu_{\text{agua}}}, 10000HU \qquad (1)$$

We use one approximate range of 3000 levels of gray which can be represented by integer

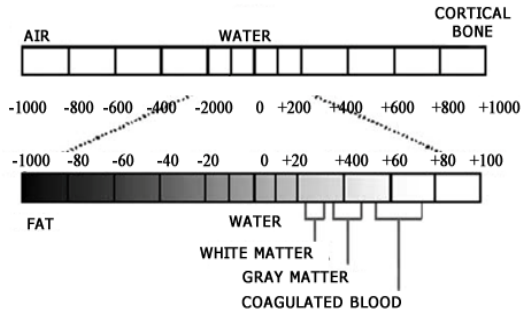

Fig. 1. Hounsfield scale

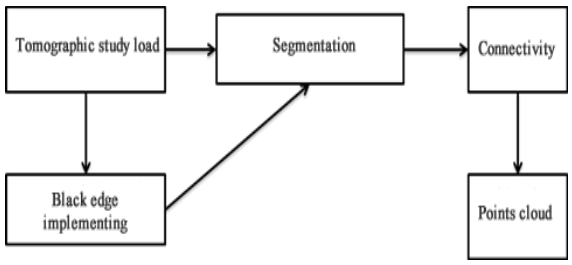

Fig. 2. Block diagram

numbers of $10^{12} = 4096$ bits. On the scale of Hounsfield, we use zero for the pixel value of the water, the air pixel with a good approximation equal to -1000 Hounsfield Unit (HU) and bone tissue between 200UH and 2000HU (Fig. 1).

We defined the range of levels of gray to work, and the image processing was performed in parallel with the algorithm whose diagram is shown in Fig. 2.

1. CT images are stored as matrices *nxn* which represent the gray value of each pixel image (Fig. 3a).
2. The value of zero is given to the tones that represent data such as air, water or soft tissues, i.e., anything that is not considered a bone.
3. We perform the calculation and histogram image.
4. We propose a first maximum and advances inside the histogram image until it produces significant and increasingly positive values. From this level it is considered as an area of interest (Fig. 3b).

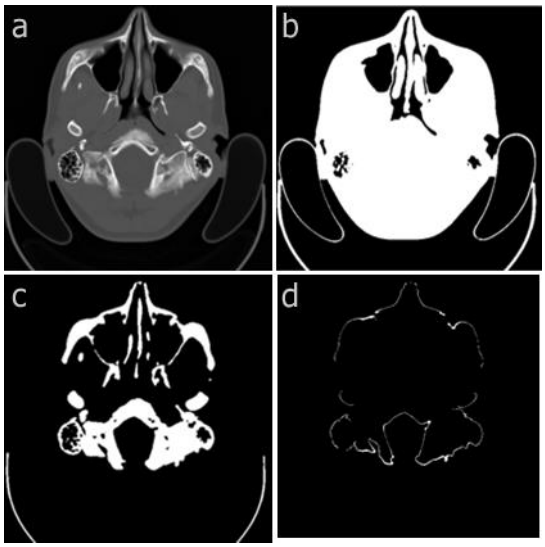

Fig. 3. Image processing

5. The resulting histogram expansion is located at the lowest level of the interest region and ponder the other levels in lineal forms.
6. A method for removing noise from the CT scan is applied to each image; this method assigns a black value to each white pixel surrounded by black pixels.

Finally, a connectivity process is implemented, which discriminates each individual structure without interest (mandible, vertebrae and patient stretcher), see Fig. 3c.

The process ends once the files are read that make up the overall 2D information (Fig. 3d).

The result is the point cloud data sets of surface cranium (Fig. 4), and with this information we built the cranium in 3D using ROOT 5.34/01 [11].

3 Interest Point Selected Methods

Two methods based on the principle of deformable models are presented below. They are neither the only nor the most powerful methods but techniques with a good tradeoff between the computational cost and the quality of segmentation. Applying the first method, called Gradient Vector Flow (GVF), we generated

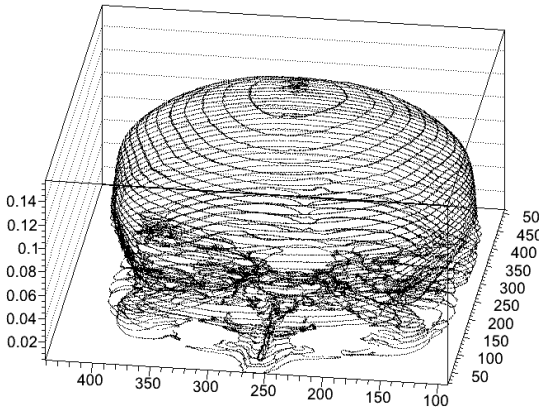

Fig. 4. Cranium in 3D

variations, so this flexibility has been a major interest for use. The second method is a consequence of the first one in terms of reducing the computation time and providing other benefits, and is known as the Vector Field Convolution (VFC).

3.1 GVF: Gradient Vector Flow

This segmentation method based on deformable models [2] improves other deformable models in two important respects. The first one is that the surface mesh is drawn to the edges of the organ of interest from farther distances, and this distance takes into account the position of the neighboring edges, which gives a second segmentation quality concavities.

First we define the gradient vector flow field to be the vector field $v(x,y) = [u(x,y), v(x,y)]$ that minimizes the energy functional

$$\varepsilon = \iint \mu\left(\mathrm{u}_\mathrm{x}^2 + \mathrm{u}_\mathrm{y}^2 + \mathrm{v}_\mathrm{x}^2 + \mathrm{v}_\mathrm{y}^2\right) + |\nabla \mathrm{f}|^2 |\mathrm{v} - \nabla \mathrm{f}|^2 \, \mathrm{dx}\, \mathrm{dy} \quad (2)$$

This variational formulation follows a standard principle of making the result smooth when there is no data. In particular, when $|\nabla f|$ is small, the energy is domatinated by sum of squares of the partial derivatives of the vector field, yielding a slowly varying field. On the other hand, when $|\nabla f|$ es large, the second term dominates the integrand and is minimized by setting $v = \nabla f$. The parameter μ is a regularization parameter governing the tradeoff between the first term and the second term in the integrand.

3.1.1 Numerical Implementation

Using the calculus of variations, it can be shown that the GVF field can be found by solving the following Euler equations:

$$\mu\nabla^2 \mathrm{u} - (\mathrm{u} - \mathrm{f_x})\left(\mathrm{f_x^2} + \mathrm{f_y^2}\right) = 0 \quad (3)$$

$$\mu\nabla^2 \mathrm{v} - \left(\mathrm{v} - \mathrm{f_y}\right)\left(\mathrm{f_x^2} + \mathrm{f_y^2}\right) = 0 \quad (4)$$

where ∇^2 is the Laplacian operator. These equations provide further intuition behind the GVF formulation. Note that in a homogeneous region (where $I(x,y)$ is constant), the second term in each equation is zero because the gradient of $f(x,y)$ is zero. Therefore, within such a region, *u* and *v* are each determined by Laplace equation, and the resulting GVF field is interpolated from the region boundary, reflecting a kind of competition among the boundary vectors. This explains why the GVF yields that point into boundary concavities.

The computational cost increases as this constant increases and it is a price that must be paid when the mesh surface initialization is far from the edges of the organ of interest.

3.2 VFC: Vector Field Convolution

Research on the computational cost of GVF led us to propose an emulation of the creation of the vector field [10]. So, the vector field is the diffusion gradient vector of the desired edges. It was proposed to create the vector field spreading with no diffusion gradient from convolution of a kernel vector, which is the initial edge of the structure of interest.

First we define a vector field kernel $k(x,y) = [u_k(x,y), u_k(x,y)]$ in which all the vectors point to the kernel origin:

$$k(x,y) = m(x,y)n(x,y) \quad (5)$$

where $m(x,y)$ is the magnitude of the vector at (x,y) and $n(x,y)$ is the unit vector pointing to the kernel origin (0, 0):

$$n(x,y) = [-\frac{x}{r}, -y/r] \quad (6)$$

except *n (0, 0) = [0, 0]* at the origin, where $r = \sqrt{x^2 + y^2}$ is the distance from the origin. If the origin is considered as the *Features of Interest* (FOI), this vector field kernel has a desirable property that a free particle placed in the field is able to move to the FOI, such as edges. Note that the kernel is origin of the structure.

The VFC field highly depends on the magnitude of the vector field kernel $m(x, y)$. By considering the fact that the influence from the FOI should decrease as the particles are further away, the magnitude should be a decreasing positive function of distance from the origin.

3.2.1 Numerical Implementation

The continuous vector field kernel $k(x, y)$ is approximated by a discrete and finite matrix given as

$$K = \{k(x, y); x, y = -R, \dots, -1,0,1, \dots, R\}$$

where *R* denotes the preferred kernel radius.

Three advantages are obtained from this segmentation method. First, the generation time of the vector field is substantially reduced by the type of transactions performed. Secondly, the vectors in the vector field point to the centers of gravity of the structure to improve the attraction concavities or stretches. And thirdly, the method is less sensitive to noise. This method is called the vector field convolution, VFC.

3.2.2 Adaptive Methods

First, a local selection of points should not involve a complete reconstruction of the structures that are modeled; in contrast, it must be local computational cost that would entail. On the other hand, the time required for modification should be proportional to the number of modified elements. To achieve these desirable objectives, it is necessary to find algorithms and data structures that conform to the structure of the problem as well as the refinement scheme used.

3.2.3 Approximation Point Method

We view this method as a constrained optimization problem. It intends to seek the surface passing through points with the minimum curvature, or with the lower gradient [4]:

$$|f(x) - f(y)| \leq K|x - y| \tag{7}$$

The minor dimension *K* which verifies the above inequality is a function of minimum variation in the direction of the gradient.

At this point the problem is to minimize the following functional form:

$$J(u) = sup_{x \in \Omega} f(x, u, D(u)) \tag{8}$$

It is defined by *u* in *W*, set of liptschitzians functions Ω bounded in R^n, where *u* represents the sought after surface and $f = \|\nabla u\|$.

The existence of solutions is guaranteed with fairly weak conditions on the function f, as quasiconvexity. Therefore, they try to follow a procedure of discretization based on finite differences. They define the discretization of Ω_k of Ω in size cells $\left(\frac{1}{p}\right) x \left(\frac{1}{p}\right)$, and to define the discretization W_k of W. We consider upper and lower triangles in $\overline{\Omega}_k$, obtaining $W_k = \{v \in W\}$, affine in every triangle.

The functions of *v* are considered as vectors, where the components are free except for the coordinates where we have data.

3.2.4 Vector Interaction Field Method

Several approaches can be considered to select the number of rings around a point as neighborhood. But in irregular and complex meshes, these methods do not approximate a neighborhood adequately.

To tackle this problem, we develop an adaptive technique. Our method selects a different neighborhood size depending on the area where the impact is applied:

$$\left|\vec{f}(\bar{x}).\, g(\bar{x})\right| < \delta \tag{9}$$

and

$$\left|\vec{f}(\bar{x}) x g(\bar{x})\right| < \delta \tag{10}$$

where $\delta > 0$.

It is important to note that our method selects a fraction of the number of interest.

4 Selecting Interest Points

As each vertex is associated with the gradient operator value, we present two ways to select the interest points of a given object. Firstly, we preserve the vertices which are local maxima. To do so, we select a vertex *v* which holds the following condition:

$$h(v) > h(w) \forall\, w \in V' | smallAng(v,w)| = k \qquad (11)$$

Secondly, we present two approaches to select the final set of interest points.

Select the points with the highest response. We can pick a constant fraction of interest points depending on the application. In this proposal, we obtain the points with higher saliency; therefore, some portions of the object do not have interest points.

The best distribution of interest points. This proposal consists of two steps. First, we sort the pre-selected interest points according to the gradient operator values in a decreasing order. Second, we apply Algorithm 1 to sorted points and select the final set of interest points.

Algorithm 1. Interest Points (Gradient Method)

Requires: Set P of pre-selected interest points in order of the gradient operator value.
Ensures: Final set of interest points.
Let Q be a set of points
$Q \leftarrow \emptyset$
for $i \leftarrow 1$ to |P| do
Gradient Method(*ρ)*
end for
Return Q

The value of *ρ* can be considered as a fraction of the percentage of the object bounding and it has effect in the number of returned interest points. Fig. 5 and Fig. 7 show the result of the two options to select interest points.

5 Cranial Deformation

The analytical models are limited to problems with regular geometry, the simple boundary condition and homogeneous properties of materials.

Problems with geometrically complex domains of materials can be represented by a collection of geometrically simple subdomains called finite elements. The approximation functions are derived for each finite element since any continuous function can be represented by a linear combination of algebraic polynomials. Head injuries are related to failure of the tissue, characterized in some form of stress, strain or deformation. Finite element method can provide distribution of stress, strain or deformation across and within different tissues of a given biomechanical input, as the impact on the cranium. Identification of the magnitudes and the location of the quantities, which exceed the tolerance level of tissues, constitutes the link between external mechanical quantities and internal injuries. Finite element models are repeatable and reproducible, and simulations may be seen as substitution experiments without biologic variability.

5.1 Finite Element Modeling (FEM)

FEM is one of the most frequently used methods for solving problems of stress-strain. This is because it is possible to predict the distribution of stresses and displacements which occur in these areas to apply loads without resorting to models in vitro. The input variables for this kind of models are:

- The mechanical properties of the materials in the case of the cranium are equal in all directions and exhibit isotropic behavior.
- Charge distributions on some items of the cranium.
- The actual geometry used three-dimensional elements and it is intended to gain a better approximation of the model, which is a better adjustment of the results obtained and greater utility in them.

Resolving the issue through the finite element method could be divided into the following phases:

$$\{\mathrm{U}\} = [\mathrm{N}]\{\mathrm{U}\} \qquad (12)$$

$$\{\epsilon\} = \left[\mathrm{N}^{\mathrm{i}}\right][\mathrm{U}] \qquad (13)$$

5.2 Geometric Discretization

A body which we call Ω is divided into *p* parts $\Omega_i..\Omega_p$ with $(\Omega_i \cap \Omega_j) = 1$ (Fig. 6), which is a non-overlapping decomposition [2].

The subdomains Ω_i are related to the processors in such a way that all computation for Ω_i are performed on the processor *i*. Thus, each subdomain can be discretized independently of other subdomains with finite element. The only constraint which one has to consider is a consistent discretization of the coupling boundaries, which means that an interface ∂i ∩ ∂k, both domains must have the same number of nodes.

5.3 Selecting Interpolation Functions

After discretizing the domain into finite elements and introducing piecewise interpolation functions, each element is defined by an interpolation function that describes the behavior between the points. Interpolation functions express Cartesian displacement $u = [u, v, w]^T$ of any point within the element in terms of displacements and strain of its nodes $a_i^e = [u_i, v_i, w_i]^T$.

The final system of equations, which results from the above approximations (1) and (2), has the form

$$[\mathrm{K}]\{\mathrm{U}\} = \{\mathrm{F}\} \tag{14}$$

where the global stiffness matrix [K] in (14) is in fact a collection of elemental stiffness matrices

$$[\mathrm{K}] = \sum_{\mathrm{i}} [\mathrm{K}^{(\mathrm{i})}] \tag{15}$$

Evaluation of the elemental stiffness matrices involves computation of interpolation functions which are local over the domain of a single finite element. The inherent parallelism (15) in the concurrent generation of the element matrices is clear.

5.4 Indicate the Properties of Elements

The properties considered were obtained from specialized literature [8, 16]; the load conditions and frontier are applied according to the final position of a stereotactic frame fixed on the human head (Table 1).

The properties are linear elastic to the cranium.

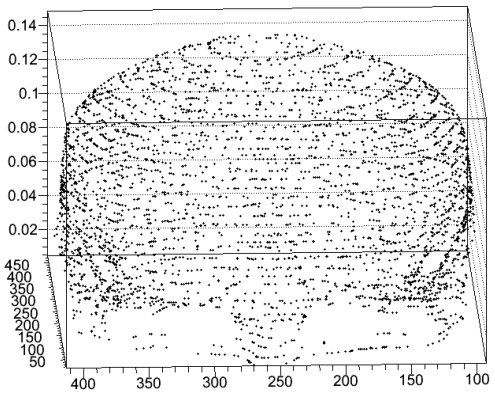

Fig. 5. Selection points from 35%

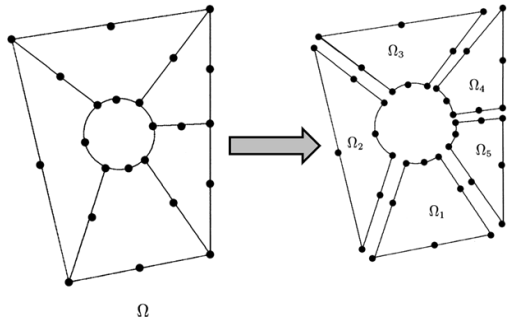

Fig. 6. Overlapping domain decomposition

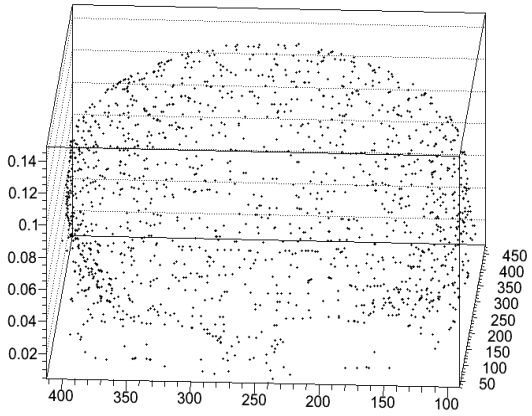

Fig. 7. Selection points from 25%

Table 1. The mechanical properties used in the numerical model

	Young's modulus P(Pa)	*mass density* E (N/mm^3)	*The Poisson ratio* ν
Cranium[8]	2019	6500	0.21
Facial bone[16]	5000	6500	0.2

5.5 Matrix Assembly

The stiffness matrix of the structure is formed of contributions from the different matrices of individual elements. This operation is referred to as assembly.

$$[\mathrm{K}]^{\mathrm{e}} = \int_{\mathrm{A}} [\mathrm{B}]^{\mathrm{T}}[\mathrm{k}][\mathrm{B}]\mathrm{tdxdy} \qquad (16)$$

It can also be expressed as a matrix called the stiffness matrix, which indicates the local properties of each element:

$$\mathrm{k}^{\mathrm{e}} = \begin{bmatrix} \mathrm{k_{ii}} & \ldots & \mathrm{k_{in}} \\ \vdots & . & \vdots \\ \mathrm{k_{ni}} & .. & \mathrm{k_{nn}} \end{bmatrix} \qquad (17)$$

In the assembly process, the coefficient k_j of the elementary matrix must be placed in the position *ij* of the overall stiffness matrix *K* of the structure.

$$[K] = \begin{pmatrix} k_{11}^e & \cdots & k_{1n}^e \\ \vdots & \ddots & \vdots \\ k_{n1}^e & \cdots & k_{nn}^e \end{pmatrix}_{nxn} \qquad (18)$$

The stiffness matrix of the element is a square matrix of *n*x*n* size, where *n* is the product of the degrees of freedom of the element by the number of nodes (*m*). For computation, the matrix is divided into *m*x*m* (number of nodes) submatrices.

The force vector of the structure considers the contribution of each element of the mesh. In the assembly process, the coefficient f_i^e must be placed in the position of the overall force vector of the structure f (Fig. 8).

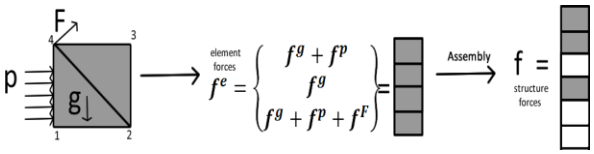

Fig. 8. Overall force vector

5.6 Geometric Reconstruction

First, we use an algorithm which allows obtaining the Delaunay triangulation for geometric reconstruction [7]. We use the point cloud data set, but the result is a mesh like one in Fig. 9, where unconvincing areas are highly dense with respect to the surface under analysis.

It is here that we apply an adaptive method for selecting points, to improve the analysis and achieve better accuracy and lower computational cost.

Thus, the original problem is transformed into a nonlinear optimization and finite-dimensional differentiable problem to be solved numerically by FEM. In particular, the processed information represents the points in a matrix and the points should be chosen to optimize the gradient norm calculated by the finite difference approximation.

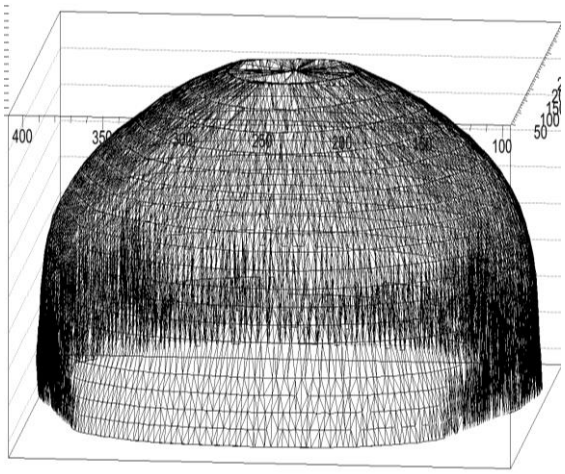

Fig. 9. Geometric cranium reconstruction

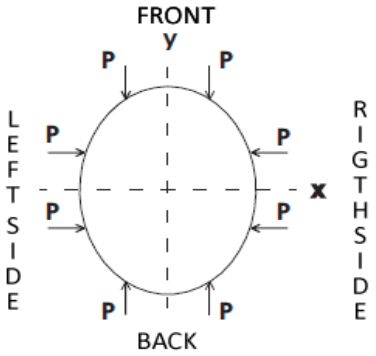

Fig. 10. Simulated strength

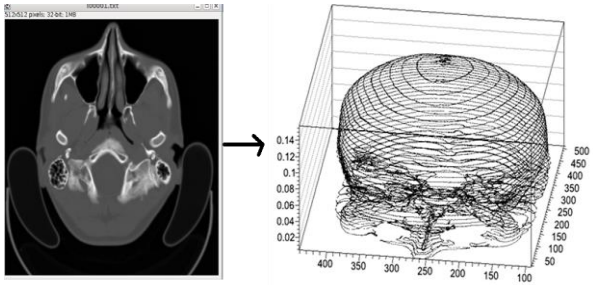

Fig. 11. Results of image processing

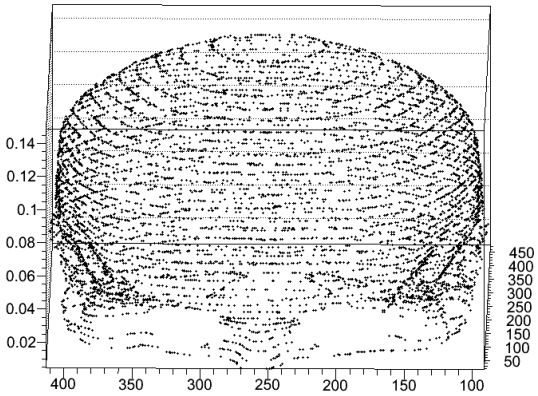

Fig. 12. Selection points from 50%

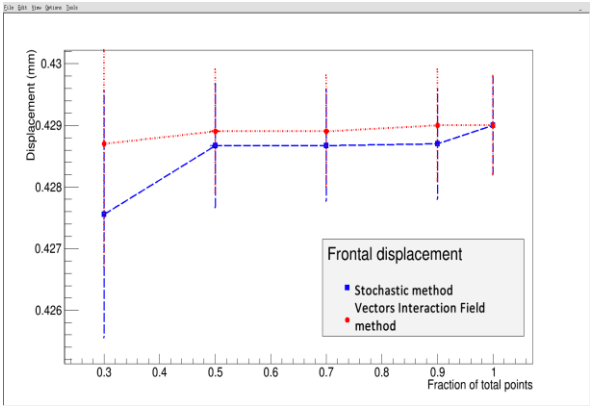

Fig. 13. Effect of reducing the number of interest points in frontal and back sides

6 Results

We applied compressive forces in the first case, two on the front and two on the back, two on the right side and two on the left side. Fig. 10 shows the simulated strength with a strength load value P = 1000N, such as in [8].

We worked with CT images and exploited the Hounsfield scale in the parallel algorithm for image processing, and this allowed us to obtain better characterization of the cranium taking into account the results presented in [8] for image processing (Fig. 11).

We performed experiments by varying average points to see the accuracy effect of reducing the number of interest points according to the two methods (the gradient method and the stochastic method), see Fig. 12.

Fig. 13 shows the displacement on the front and back sides, obtained with a strength load value P = 1000N and using different point cloud. Fig. 14 shows the displacement on the left and right sides, obtained with a strength load value P = 1000 N and using different point cloud.

7 Conclusions

We presented a new point selection method. The performance characteristics of the structure with a uniform number of points do not affect the convergence of the method and decrease the speed of convergence. This is why the tests were conducted with a smaller number of points and were analyzed with a lower computational cost and better approximation.

In addition, from the results obtained with our method, the experiments confirm that the numerical solutions are limited by density and quality of discretization.

Furthermore, the performed experiments show that our method can be used with good results for 2D and 3D structures.

Acknowledgments

This project is funded by CONACYT (Mexico) through a Doctoral Scholarship.

References

1. **Wohlmuth, B.I. (2001).** *Discretization Methods and Iterative Solvers Based on Domain Decomposition*. Berlin; New York: Springer.
2. **Li, B. & Acton, S.T. (2007).** Active Contour External Force using Vector Field Convolution for Image Segmentation. *IEEE Transactions on Image Processing*, 16(8), 2096–2106.
3. **Bolle, R.M. & Vemuri, B.C. (1991).** On Three Dimensional Surface Reconstruction Methods. *IEEE Transactions on Pattern Analysis and Machine Intelligence*, 13(1), 1–13.
4. **C. García Bauza, V. Cifuentes (2010)**, "Método del punto proximal para la reconstrucción automática de geometría de lechos", Mecánica computacional.
5. **Gelfand, N., Mitra, N.J., Guibas, L.J., & Pottmann, H. (2005).** Robust global registration. *Third Eurographics Symposium on Geometry Processing*, Vienna, Austria, Article No. 197.
6. **Hu, J. & Hua, J. (2009).** Salient spectral geometric features for shape matching and retrieval. *The Visual Computer: International Journal of Computer Graphics, 25*(5-7), 667–675.
7. **Hoffmann, C.M. (1989).** *Geometric and Solid Modeling: an introduction*. San Mateo, Calif.: Morgan Kauffmann.
8. **Nieto, J.J., Minor, A., Álvarez, J., Alonso, M.A., & Algorri, M.E. (2005).** Análisis de esfuerzos de compresión en el cráneo humano por medio del método del elemento finito. *Revista Mexicana de Ingeniería Biomédica*, 26(1), 16–21.
9. **Lee, C.H., Varshney, A., & Jacobs, D.W. (2005).** Mesh saliency. *32nd International Conference on Computer Graphics and Interactive Techniques (SIGGRAPH 2005)*, Los Angeles, CA, 659–666.
10. **Li, B. & Acton, S.T. (2007).** Active Contour External Force Using Vector Field Convolution for Image Segmentation. *IEEE Transactions on Image Processing*, 16(8), 2096–2106.
11. Root (2013). Retrieved from http://root.cern.ch/drupal/.
12. **Tierny, J., Vandeborre, J.P., & Daoudi, M. (2008).** Enhancing 3D mesh topological skeletons with discrete contour constrictions. *The Visual Computer: International Journal of Computer Graphics*, 24(3), 155–172.
13. **Wriggers, P. & Boersma, A. (1998).** A parallel algebraic multigrid solver for problems in solid mechanics discretized by Finite elements. *Computers & Structures,* 69(1), 129–137.
14. **Venere M. y Dari E. (2012).** Análisis comparativo de algoritmos para obtener triangulaciones Delaunay. *Mecánica Computacional*, 10, 491-506.
15. **Gropp, W., Lusk, E., & Skjellem, A. (1999).** *Using MPI, Portable Parallel Programming Whit the Message-Passing Interface* (*2nd ed*.). Cambridge, Mass.: MIT Press.
16. **Willinger, R., Kang, H.S., & Diaw, B. (1999).** Three-dimensional human head finite-element model validation against two experimental impacts. *Annals of Biomedical Engineering,* 27(3), 403–410.
17. **Xu, C. & Prince, J.L. (1998).** Snakes, shapes, and gradient vector flow. *IEEE Transactions on Image Processing*, 7(3), 359–369.
18. **Katz, S., Leifman, G., & Tal, A. (2005).** Mesh segmentation using feature point and core extraction. *The visual Computer,* 21(8-10), 649–658.
19. **McInerney, T. & Terzoupoulos, D. (1999).** Topology adaptive deformable surfaces for medical image volume segmentation. *IEEE Transactions on Medical Imaging*, 18(10), 840–850.
20. **McInerney, T. & Terzoupoulos, D. (1996).** Deformable models in medical image analysis: A survey. *Medical Image Analysis,* 1(2), 91–108.
21. **Cootes, T.F., Edwards, G.J., & Taylor. C.J. (2001).** Active appearance models. *IEEE Transactions on Pattern Analysis and Machine Intelligence,* 23(6), 681–685.

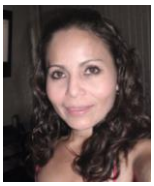

Claudia García-Blanquel is a Ph.D. student of the Artificial Intelligence Laboratory of the Computing Research Center of National Polytechnic Institute of Mexico. She has a Master's degree in Computer Science. Her research interests include parallel programming, GRID computing, HPC, scientific computing, modeling and simulation.

Amit Majumdar is the director of the Scientific Computing Applications Group at the San Diego Supercomputer Center and an associate professor in the Department of Radiation Medicine and Applied Sciences at the University of California, San Diego. He has an M.S. in Nuclear Engineering and Mathematics, and a Ph.D. in the interdisciplinary field of Nuclear Engineering and Scientific Computing. His research interests are performance analysis of HPC codes, utilization of HPC for medical applications and science gateways providing access to cyber infrastructure for domain scientists.

René Luna-García is a professor at the Artificial Intelligence Laboratory of the Computing Research Center of National Polytechnic Institute of Mexico. He is a member of High Altitude Water Cherenkov Experiment for Cosmic Rays. He has a Master's degree in Nuclear Physics and a Ph. D. in Cosmic Rays. He did his postdoctoral research at the DZERO-TEVATRON Particle Accelerator at Fermi Lab as part of diffraction group. He has more than 200 papers with the DZERO collaboration. His research interests include high energy physics, cosmic rays, modeling, simulation, and scientific computing.

Article received on 11/02/2013; accepted on 11/08/2013.